Available online at www.sciencedirect.com
SCIENCE DIRECT®
International Journal of Thermal Sciences 42 (2003) 209–222
International Journal of Thermal Sciences
www.elsevier.com/locate/ijts

Transient coupled heat transfer in a multi-layer composite with opaque specular surfaces and semitransparent specular interfaces

He-Ping Tan, Jian-Feng Luo *, Li-Ming Ruan, Qi-Zheng Yu

Harbin Institute of Technology, School of Energy Science and Engineering, 92 West Dazhi Street, Harbin 150001, People's Republic of China

Received 24 September 2001; accepted 18 March 2002

Abstract

In this paper, one-dimensional transient coupled radiative and conductive heat transfer in a multi-layer absorbing and isotropic scattering composite is investigated. The composite is considered to be of opaque specular boundaries and semitransparent specular interfaces. In combination with ray tracing method, spectral band model and the Hottel and Sarofim's zonal method, the radiative transfer coefficients (RTCs) of the multi-layer composite are deduced. The RTCs are used to calculate the radiative heat source term in the transient energy control equation, which is solved by the fully implicit discrete control-volume method. The effects of refractive index and vacuum space on transient coupled heat transfer are analyzed. Except for refractive index, all the other parameters of each layer have been kept the same, and the total thickness also has been kept unchanged, then along the thickness of the composite when the decrement or the increment of refractive index decreases as layer number increases, the temperature profile becomes smoother and the steady heat flux increases.

Keywords: Composite; Radiation; Conduction; Transient

1. Introduction

Semitransparent medium has found applications in many industry fields, such as the insulating techniques for the protection of aeroengines [1,2] and the processing of glass products [3–6] etc. Many papers investigated coupled radiative and conductive heat transfer in a single planar semitransparent slab [3–12]. As the layer number of a composite increases, interactions among all layers and reflection, especially total reflection at all the interfaces, become very complex. In Refs. [13–16], the coupled heat transfer in a two-layer semitransparent composite is investigated. The studies of coupled heat transfer in multi-layer composite [17–19] are relatively much less than those in one-layer medium and two-layer composite. In early 1986, Tsai et al. [17] and Timoshenko et al. [18], respectively studied the transient coupled radiative and conductive heat transfer in a multi-layer absorbing-emitting composite. In Ref. [17], all of the interfaces and surfaces are supposed to be opaque and gray, so each layer cannot directly exchange radiative energy with other layers. In Ref. [18], the interfaces are composed of very thin coatings, which absorb, reflect, and also transmit radiation inside the layer in an isotropic manner. In 1993, neglecting the heat conduction, Siegel and Spuckler [19] studied the effect of refractive index on radiative heat transfer in a multi-layer absorbing, isotropically scattering composite, and all the interfaces and surfaces of the composite are semitransparent and diffuse. Fresnel's reflective law and Snell's refractive law are used to determine the mean reflectivity of diffuse interface.

In above papers, only Refs. [3,4,8] studied specular reflection, and much more papers considered diffuse reflection. So far, a paper that investigated coupled heat transfer in multi-layer composite with semitransparent and specular interfaces has not been found yet. In this paper, based on Refs. [20] and [21], which investigated the transient coupled heat transfer in a three-layer composite with semitransparent and specular interfaces, the multi-layer transient coupled heat transfer is investigated by the ray tracing/node analyzing method. The transient coupled heat transfer model put forward here is with respect to a multi-layer absorbing, isotropically scattering composite with opaque specular boundaries and semitransparent specular interfaces. The difference between diffuse reflectivity and specular reflec-

* Corresponding author.
E-mail addresses: luo_ jianfeng@yahoo.com (J.-F. Luo), ruanlm@hope.hit.edu.cn (L.-M. Ruan).

1290-0729/02/$ – see front matter
PII: S1290-0729(02)00022-4

Nomenclature

Abbreviations

RTC radiative transfer coefficient, such as $(V_iV_j)_k$ and $[S_uS_v]_k$ etc.

$a1, a2$ surface, interface or control volume, used to define one-layer radiative intensity quotient transfer function

$b1, b2$ surface or interface, used to define multi-layer radiative intensity quotient transfer function

c_b specific heat capacity of bth layer ..... $\mathrm{J\cdot kg^{-1}\cdot K^{-1}}$

E_n $E_n(x) = \int_0^1 \mu^{n-2}\exp(-x/\mu)\,\mathrm{d}\mu$

$\boldsymbol{F}$ radiative intensity quotient transfer function of one-layer semitransparent medium model

$\boldsymbol{H}$ radiative intensity quotient transfer function of multi-layer semitransparent medium model

I_b Ith node in bth layer

h_1, h_2 convective heat transfer coefficients at surfaces S_1 and S_2, respectively ..... $\mathrm{W\cdot m^{-2}\cdot K^{-1}}$

k_b thermal conductivity of bth layer of medium ..... $\mathrm{W\cdot m^{-1}\cdot K^{-1}}$

k_{ie}, k_{iw} harmonic mean thermal conductivity at interface ie and iw ..... $\mathrm{W\cdot m^{-1}\cdot K^{-1}}$

L_b thickness of bth layer ..... m

L_t total thickness of composite, $= L_1 + L_2 + \cdots + L_n$ ..... m

M_b number of control volumes of bth layer

M_t total number of control volumes of composite, $= M_1 + M_2 + \cdots + M_n$

n total number of layers of multi-layer composite (Fig. 1)

$n_{b,k}$ spectral refractive index of bth layer

$n'_{i,k}$ refractive index of ith control volume; when $i \leqslant M_1$, $n'_{i,k} = n_{1,k}$; when $M_1 + M_2 + \cdots + M_{b-1} < i \leqslant M_1 + M_2 + \cdots + M_b$, $n'_{i,k} = n_{b,k}$

n_0, n_{n+1} refractive indexes of the surroundings (equal to the refractive index of air n_g, Fig. 1)

N_b conduction-radiation parameter of bth layer, $= k_b/(4\sigma T_r^3 L_t)$

NB total number of spectral bands

P_b interface between bth layer and $(b+1)$th layer; side of interface P_b facing towards bth layer

$P_{b'}$ side of interface P_b facing towards $(b+1)$th layer

q^c, q^r thermal conductive, radiative and convective

q^{cv} heat fluxes, respectively ..... $\mathrm{W\cdot m^{-2}}$

q^t total heat flux, $q^c + q^r$ ..... $\mathrm{W\cdot m^{-2}}$

$\tilde{q}$ dimensionless heat flux, $= q/(\sigma T_r^4)$

$S_{-\infty}, S_{+\infty}$ left and right black surfaces representing the surroundings (Fig. 1)

S_1, S_2 boundary surfaces (Fig. 1)

S_u, S_v surfaces, $u, v = 1$, or 2

T absolute temperature ..... K

T_0 uniform initial temperature ..... K

T_r reference temperature ..... K

T_{g1}, T_{g2} gas temperature for convection at $x = 0$ and L_t, respectively ..... K

T_{S_1}, T_{S_2} temperature of boundary surfaces S_1 and S_2, respectively ..... K

$T_{-\infty}, T_{+\infty}$ temperatures of the black surface $S_{-\infty}$ and $S_{+\infty}$, respectively (Fig. 1) ..... K

t physical time ..... s

t^* dimensionless time, $= t4\sigma T_r^3/(\rho_1 c_1 L_t)$

V_i ith control volume, $i = 1$ to M_t

V_{I_b} Ith control volume of bth layer, $I = 1$ to M_b

$(V_iV_j)_k, [V_iV_j]_k$ parts of radiative energy emitted by V_i at the kth spectral band $(\Delta\lambda_k)$ and arriving at V_j for non-scattering and scattering media, respectively

$(S_uS_v)_k, [S_uS_v]_k$ parts of radiative energy emitted by S_u at the kth spectral band $(\Delta\lambda_k)$ and arriving at S_v for non-scattering and scattering media, respectively

$(S_uV_j)_k, [S_uV_j]_k$ parts of radiative energy emitted by S_u at the kth spectral band $(\Delta\lambda_k)$ and arriving at V_j for non-scattering and scattering media, respectively

$(V_iS_v)_k, [V_iS_v]_k$ parts of radiative energy emitted by V_i at the kth spectral band $(\Delta\lambda_k)$ and arriving at S_v for non-scattering and scattering media, respectively

x coordinate in direction across layer ..... m

x_i, y_i geometrical progressions used in tracing radiative intensity's transferring

x_a^b distance between surface a and b ..... m

X dimensionless coordinate in direction across layer, $= x/L_t$

$\alpha_{b,k}$ spectral absorbing coefficient of bth layer $\mathrm{m^{-1}}$

Γ attenuated quotient of radiative intensity by control volume or surface (Eq. (7))

$\gamma(\theta)_{bo}$ transmissivity of radiative intensity propagating from layer "b" to layer "o" at angle θ, $= 1 - \rho(\theta)_{bo}$

Δx_b control volume thickness of bth layer ..... m

Δt time step ..... s

Δt^* dimensionless time step

$(\delta x)_{ie}, (\delta x)_{iw}$ distance between nodes i and $i+1$, and that between nodes i and $i-1$, respectively (Fig. 1) ..... m

$\varepsilon_{0,k}\varepsilon_{1,k}$ emissivities of the outside and inside of surface S_1

$\varepsilon_{2,k}\varepsilon_{3,k}$ emissivities of the inside and outside of surface S_2

η_b $= 1 - \omega_b$

η'_i $= 1 - \omega'_i$

Θ	dimensionless temperature, $= T/T_r$
θ'_{ij}	critical angle, $\arcsin(n_j/n_i)$, if $n_i > n_j$
$\kappa_{b,k}$	extinction coefficients of bth layer, $\alpha_{b,k} + \sigma_{s,b,k}$ ..... m^{-1}
ρ_b	density of bth layer ..... $\mathrm{kg{\cdot}m^{-3}}$
$\rho(\theta)_{bo}$	reflectivity of intensity going from layer "b" to layer "o" at angle θ
$\sigma_{s,b,k}$	spectral scattering coefficient of bth layer. m^{-1}
$\tau_{b,k}$	spectral optical thickness of bth layer, $= \kappa_{b,k} L_b$
Φ_i^r	radiative heat source of control volume i
$\omega_{b,k}$	spectral scattering albedo of bth layer, $= \sigma_{s,b,k}/\kappa_{b,k}$
$\omega'_{i,k}$	spectral scattering albedo of ith control volume; when $i \leqslant M_1$, $\omega'_{i,k} = \omega_{1,k}$; when $M_1 + M_2 + \cdots + M_{b-1} < i \leqslant M_1 + M_2 + \cdots + M_b$, $\omega'_{i,k} = \omega_{b,k}$

Superscripts

m	time step
s	specular reflection
$*$	normalized values

Subscripts

a, b	layer index, $a, b = 1$ to n
bo	intensity propagating from layer "b" to layer "o"
c	cth layer, either b or o layer
g	gas (air)
i, j	relative to nodes; index of geometrical progression term
k	relative to spectral band k
o	oth layer, either $b-1$ or $b+1$ layer
$o{-}o$	refers to a composite with opaque surfaces
S_1, S_2	relative to S_1 and S_2
u, v	1 or 2
va	relative to vacuum space
$-\infty, +\infty$	relative to $S_{-\infty}$ and $S_{+\infty}$
$//, \perp$	relative to component for parallel and perpendicular polarization, respectively

tivity at semitransparent interface is that diffuse reflectivity does not depend on incident direction, but specular reflectivity does. For diffuse semitransparent interface total reflection is considered in diffuse reflectivity, as used in Refs. [16] and [19]. But for specular semitransparent interface, total reflection occurs when the incident angle is greater than the critical angle. For a multi-layer composite with semitransparent specular interfaces, the arrangement of refractive indexes among all layers is arbitrary, so the total reflections at all interfaces are very complex, and a proper method is used here to deal with this problem.

For specular reflection, the unpolarized radiative intensity can be divided into two equal parallel and perpendicular components and be traced separately. Corresponding to these two components the reflectivity of an interface is classified as parallel and perpendicular, and Fresnel's reflective law and Snell's refractive law are used to determine the specular reflectivity [8], as shown in Appendix A.

2. Physical model and discrete governing equation

As shown in Fig. 1, a composite of n-layer planar absorbing, isotropically scattering semitransparent medium is located between two black surfaces $S_{-\infty}$ and $S_{+\infty}$. The surfaces S_1 and S_2 are opaque (with coatings). The interfaces of the composite, $P_1, P_2, \ldots,$ and P_{n-1}, are semitransparent and specular. Along the thickness, the n layers are divided into $M_1, M_2, \ldots,$ and M_n control volumes (inner nodes), respectively, and I_b is used to denote the Ith nodes in the bth layer, and for convenience, all nodes are also denoted

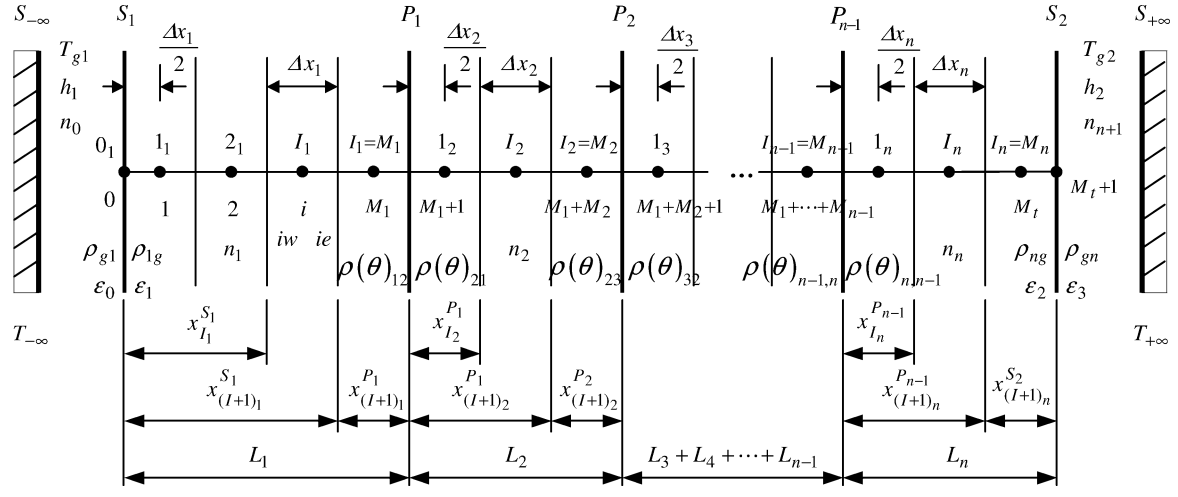

Fig. 1. Physical model of a n-layer semitransparent composite with opaque specular boundaries and semitransparent interfaces.

by i increasingly along the whole thickness. If $b = 1$, then $i = I_b$, else $i = M_1 + M_2 + \cdots + M_{b-1} + I_b$.

The variation of the medium spectral properties with wavelength, such as κ_b, α_b, and n_b etc., can be approximately expressed by a series of rectangular spectral bands.

The fully implicit discrete energy equation of the ith control volume in the bth layer is [20,21]

$$\rho_b c_b \Delta x_b \frac{T_i^{m+1} - T_i^m}{\Delta t} = \frac{k_{ie}^{m+1}(T_{i+1}^{m+1} - T_i^{m+1})}{(\delta x)_{ie}} - \frac{k_{iw}^{m+1}(T_i^{m+1} - T_{i-1}^{m+1})}{(\delta x)_{iw}} + \Phi_i^{r,m+1} \tag{1}$$

As shown in Appendix B, the radiative heat source term Φ_i^r in Eq. (1) can derived as:

$$\begin{aligned}\Phi_i^r = \sigma \sum_{k=1}^{NB} \Bigg\{ \sum_{j=1}^{M_t} \big\{ & n_{j,k}'^2 [V_j V_i]_{k,o-o}^s A_{k,T_j} T_j^4 - n_{i,k}'^2 [V_i V_j]_{k,o-o}^s A_{k,T_i} T_i^4 \big\} \\ & + \big\{ n_{M_t,k}'^2 [S_2 V_i]_{k,o-o}^s A_{k,T_{S_2}} T_{S_2}^4 - n_{i,k}'^2 [V_i S_2]_{k,o-o}^s A_{k,T_i} T_i^4 \big\} \\ & + \big\{ n_{1,k}'^2 [S_1 V_i]_{k,o-o}^s A_{k,T_{S_1}} T_{S_1}^4 - n_{i,k}'^2 [V_i S_1]_{k,o-o}^s A_{k,T_i} T_i^4 \big\} \Bigg\} \\ & 1 \leqslant i \leqslant M_t \end{aligned} \tag{2}$$

When $i = M_t + 1$, the radiative heat flux at surface S_2 is

$$\begin{aligned} q_{S_2}^r = \sigma \sum_{k=1}^{NB} \Bigg\{ \sum_{j=1}^{M_t} \big\{ & n_{j,k}'^2 [V_j S_2]_{k,o-o}^s A_{k,T_j} T_j^4 - n_{M_t,k}'^2 [S_2 V_j]_{k,o-o}^s A_{k,T_{S_2}} T_{S_2}^4 \big\} \\ & + n_{1,k}'^2 [S_1 S_2]_{k,o-o}^s A_{k,T_{S_1}} T_{S_1}^4 - n_{M_t,k}'^2 [S_2 S_1]_{k,o-o}^s A_{k,T_{S_2}} T_{S_2}^4 \Bigg\} \end{aligned} \tag{3}$$

When $i = 0$, the expression of the radiative heat flux at surface S_1 is similar to Eq. (3).

The sum of radiation and conduction to surface S_2 from inside the composite medium is equal to the sum of radiation and convection leaving the outside of surface S_2, i.e.,

$$q_{S_2}^r + 2k_n(T_{M_t} - T_{S_2})/\Delta x_n = h_2(T_{S_2} - T_{g2}) + \sigma \sum_{k=1}^{NB} n_{n+1}^2 \varepsilon_{3,k} \big(A_{k,T_{S_2}} T_{S_2}^4 - A_{k,T_{+\infty}} T_{+\infty}^4 \big) \tag{4}$$

The discrete boundary condition at surface S_1 is similar to above equation.

3. RTCs of an n-layer composite with opaque and specular surfaces

The radiation transfer process in scattering semitransparent medium can be divided into two sub-processes [22]: (1) emitting–attenuating–reflecting sub-process, in which only emitting, attenuating of the medium and multiple reflecting of the interfaces are considered, and the RTCs are denoted by $(S_1 V_{I_b})_{o-o,k}^s$ etc. (2) absorbing–scattering sub-process; after considering scattering the radiative energy represented by the RTCs, $(S_1 V_{I_b})_{o-o,k}^s$ etc., will be redistributed, and the RTCs are denoted by $[S_1 V_{I_b}]_{o-o,k}^s$ etc. All the RTCs of the emitting–attenuating–reflecting sub-process satisfy the following relationship:

$$\begin{aligned} n_{1,k}^2 (S_1 S_2)_{k,o-o}^s &= n_{n,k}^2 (S_2 S_1)_{k,o-o}^s \\ n_{1,k}^2 (S_1 V_{I_b})_{k,o-o}^s &= n_{b,k}^2 (V_{I_b} S_1)_{k,o-o}^s \\ n_{n,k}^2 (S_2 V_{I_b})_{k,o-o}^s &= n_{b,k}^2 (V_{I_b} S_2)_{k,o-o}^s \\ n_{a,k}^2 (V_{I_a} V_{I_b})_{k,o-o}^s &= n_{b,k}^2 (V_{I_b} V_{I_a})_{k,o-o}^s \end{aligned} \tag{5}$$

where subscripts "a" and "b" denote the ath and the bth layer respectively, and $a, b = 1$ to n.

3.1. Multi-layer intensity transfer model for emitting–attenuating–reflecting sub-process

For specular reflection we can study the transfer process of radiative intensity in the composite by tracing it. Multi-layer radiative intensity quotient transfer functions are used here to trace radiative intensity transferring in the n-layer composite. For convenient, the two sides of an interface should be specified. Assume P_m to be the interface between the mth and the $(m+1)$th layers, then the side of the interface facing towards the mth layer is specified as P_m, and that facing towards the $(m+1)$th layer is denoted by $P_{m'}$.

The one-layer radiative intensity quotient transfer functions, expressed by symbol $\boldsymbol{F}_{a1_{b,k}}^{a2_b}$, are shown in Appendix A. Seeing Fig. 2, the multi-layer radiative intensity quotient transfer functions are expressed by symbol $\boldsymbol{H}_{b1,m+1\sim m+\Delta m,k}^{b2}$, which means the total quotient of the spectral radiative intensity arrived at superscript $b2$ (represents $P_{m'}$, $P_{m+1'}$, $P_{m+\Delta m-1}$ or $P_{m+\Delta m}$) to that emitted by subscript $b1$ (represents $P_{m'}$ or $P_{m+\Delta m}$) at kth spectral band after "transferring once" within the multi-layer model, where subscript $m+1 \sim m+\Delta m$ denotes the multi-layer model is composed of from the $(m+1)$th to the $(m+\Delta m)$th layers. The "transferring once" means the process that the radiative intensity is attenuated and reflected repeatedly until it becomes 0 within the layers considered in the model.

Take $\boldsymbol{H}_{P_{m'},m+1\sim m+\Delta m,k}^{P_{m'}}$ as an example to illustrate the deductive process of multi-layer radiative intensity quotient transfer functions, and for convenience, subscript k is omitted. See Fig. 2:

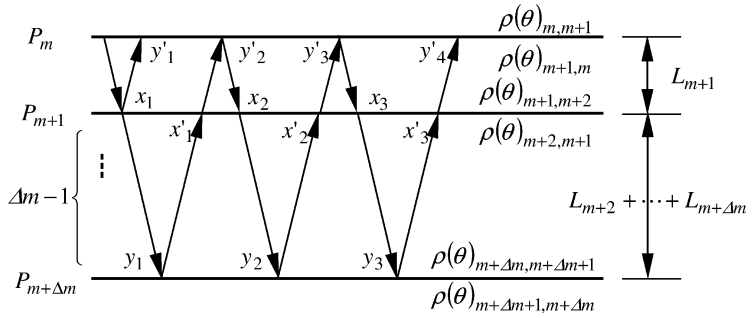

Fig. 2. Multi-layer radiative intensity transfer model.

(1) After "transferring once" within the $(m+1)$th layer, the quotient of radiative intensity arriving at $P_{m'}$ to that emitted by $P_{m'}$ for the first time is $y'_1 = \boldsymbol{F}^{P_{m'}}_{P_{m'}}$, and a quotient of $x_1 (= \boldsymbol{F}^{P_{m+1}}_{P_{m'}})$ arrives at P_{m+1}.

(2) A fraction, $\gamma(\theta)_{m+1,m+2}$, of the above quotient that arrives at P_{m+1} enters the following $\Delta m - 1$ layers, and after "transferring once" within the $\Delta m - 1$ layers, the quotient arriving at $P_{m+1'}$ for the first time is $x'_1 = x_1\gamma(\theta)_{m+1,m+2}\boldsymbol{H}^{P_{m+1'}}_{P_{m+1'},m+2\sim m+\Delta m}$. Only a part, $\gamma(\theta)_{m+2,m+1}$, of x'_1 enters the $(m+1)$th layer, and then after "transferring once" within this layer, the quotient arriving at $P_{m'}$ for the second time is $y'_2 = x'_1\gamma(\theta)_{m+2,m+1}\boldsymbol{F}^{P_{m'}}_{P_{m+1}}$. In addition, a fraction, $x_2 = x'_1\gamma(\theta)_{m+2,m+1}\boldsymbol{F}^{P_{m+1}}_{P_{m+1}}$, arrives at P_{m+1} for the second time.

(3) The above quotient x_2 repeats step (2), then the quotient arriving at $P_{m'}$ for the third time is $y'_3 = x'_2 \times \gamma(\theta)_{m+2,m+1}\boldsymbol{F}^{P_{m'}}_{P_{m+1}}$ and that arriving at P_{m+1} for the third time is $x_3 = x'_2\gamma(\theta)_{m+2,m+1}\boldsymbol{F}^{P_{m+1}}_{P_{m+1}}$, where

$$x'_2 = x_2\gamma(\theta)_{m+1,m+2}\boldsymbol{H}^{P_{m+1'}}_{P_{m+1'},m+2\sim m+\Delta m}$$

Trace the radiative intensity by this way until it finally attenuates to 0. Here, $y'_2, y'_3, y'_4, \ldots$, is an infinite geometric series with a common ratio of

$$\beta_2 = \gamma(\theta)_{m+2,m+1}\boldsymbol{F}^{P_{m+1}}_{P_{m+1}}\gamma(\theta)_{m+1,m+2}\boldsymbol{H}^{P_{m+1'}}_{P_{m+1'},m+2\sim m+\Delta m}$$

($\beta_2 < 1$). From the analysis above, the total quotient of the radiative intensity finally arriving at $P_{m'}$ to that emitted by $P_{m'}$ can be calculated as follows.

$$\begin{aligned}\boldsymbol{H}^{P_{m'}}_{P_{m'},m+1\sim m+\Delta m} &= \sum_{i=1}^{\infty} y'_i = \boldsymbol{F}^{P_{m'}}_{P_{m'}} + y'_2/(1-\beta_2)\\ &= \boldsymbol{F}^{P_{m'}}_{P_{m'}} + \big[\boldsymbol{F}^{P_{m+1}}_{P_{m'}}\gamma(\theta)_{m+1,m+2}\\ &\qquad \times \boldsymbol{H}^{P_{m+1'}}_{P_{m+1'},m+2\sim m+\Delta m}\gamma(\theta)_{m+2,m+1}\boldsymbol{F}^{P_{m'}}_{P_{m+1}}\big]\\ &\quad \times \big[1-\gamma(\theta)_{m+2,m+1}\boldsymbol{F}^{P_{m+1}}_{P_{m+1}}\gamma(\theta)_{m+1,m+2}\\ &\qquad \times \boldsymbol{H}^{P_{m+1'}}_{P_{m+1'},m+2\sim m+\Delta m}\big]^{-1} \qquad (6)\end{aligned}$$

As shown in Eq. (6), $\boldsymbol{H}^{P_{m'}}_{P_{m'},m+1\sim m+\Delta m}$ can be calculated from $\boldsymbol{H}^{P_{m+1'}}_{P_{m+1'},m+2\sim m+\Delta m}$, so Eq. (6) is a recursive expression. Therefore, the calculation should be started from the $(m+\Delta m)$th layer at first, i.e., $\boldsymbol{H}^{P_{m+\Delta m-1'}}_{P_{m+\Delta m-1'},m+\Delta m} = \boldsymbol{F}^{P_{m+\Delta m-1'}}_{P_{m+\Delta m-1'}}$. Based on this formulation and in combination with the one-layer radiative intensity quotient transfer functions $\boldsymbol{F}$ of the $(m+\Delta m-1)$th layer, the quotient $\boldsymbol{H}^{P_{m+\Delta m-2'}}_{P_{m+\Delta m-2'},m+\Delta m-1\sim m+\Delta m}$ can be evaluated from Eq. (6). Similarly, by combining the Eq. (6) with the one-layer radiative intensity quotient transfer functions $\boldsymbol{F}$ of the $(m+\Delta m-2)$th layer, $\boldsymbol{H}^{P_{m+\Delta m-3'}}_{P_{m+\Delta m-3'},m+\Delta m-2\sim m+\Delta m}$ can be evaluated. So, repeating the calculations, finally the quotient $\boldsymbol{H}^{P_{m'}}_{P_{m'},m+1\sim m+\Delta m}$ can be evaluated.

It should be emphasized that corresponding to the parallel and the perpendicular components, the values of Eq. (6) are different because the reflectivities for the two components are different. The expressions of $\rho(\theta)$ for the two components can be found in Appendix A of Ref. [20] and Ref. [21].

3.2. RTCs of an n-layer composite for emitting–attenuating–reflecting sub-process

Resorting to the multi-layer radiative intensity quotient transfer function $\boldsymbol{H}$, the RTCs of an n-layer absorbing-emitting composite ($\kappa_k = \alpha_k$) can be deduced conveniently. For example, the total quotient of the radiative intensity emitted by S_1 at the kth spectral band and finally absorbed by S_1 after "transferring once" within the n layers can be expressed as

$$\Gamma = \boldsymbol{H}^{S_1}_{S_1,1\sim n,k} \qquad (7)$$

where, the quotient Γ in Eq. (7) is relative to one of the two polarized components. So for an unpolarized radiative intensity, the final quotient absorbed by S_1 is

$$(\Gamma_{//} + \Gamma_{\perp})/2 \qquad (8)$$

By integrating expression (8) over the hemispherical space and simultaneously considering the inside emissivity of S_1, the RTC $(S_1S_1)^s_{k,o-o}$ can be solved.

The value of $\rho(\theta)$ will be one if total reflection occurs, so, due to the effect of the total reflection, Eq. (8) is not a continuous function over the whole hemispherical space, and it cannot be integrated directly over the whole

hemispherical space. To solve this problem, the following method is applied.

(1) Solve the critical angle θ'_{1b} of S_1 vs. the bth layer. If $n_1 > n_b$ ($b = 1$ to n), then $\theta'_{1b} = \arcsin(n_b/n_1)$, otherwise, $\theta'_{1b} = \pi/2$. For $b = 1$ to n, n angles can be obtained, which are $\theta'_{11}, \theta'_{12}, \theta'_{13}, \ldots$, and θ'_{1n}, and θ'_{11} must equal $\pi/2$.

(2) Then arrange these angles from small to big, and a new array can be obtained: $(\theta_{10} =)0 < \theta_{11} \leqslant \theta_{12} \leqslant \theta_{13} \leqslant \cdots \leqslant \theta_{1n}$, where θ_{1n} must equal to $\pi/2$.

After doing this, the whole hemispherical space can be divided into n intervals which are signed by these critical angels: $[\theta_{10}, \theta_{11}], [\theta_{11}, \theta_{12}], [\theta_{12}, \theta_{13}], \ldots,$ and $[\theta_{1(n-1)}, \theta_{1n}]$. And for each integrating interval, function Γ becomes continuous. So by integrating Eq. (8) within each interval and adding those results, the RTC $(S_1S_1)^s_{k,o-o}$ can be obtained:

$$(S_1S_1)^s_{k,o-o} = \varepsilon_1 \sum_{b=0}^{n-1} \int_{\theta_{1b}}^{\theta_{1(b+1)}} f(\theta)\,\mathrm{d}\theta \tag{9}$$

Where $f(\theta) = (\Gamma_{//} + \Gamma_{\perp})\cos\theta\sin\theta$.

Thus, similarly to above by using the multi-layer radiative intensity quotient transfer function $\boldsymbol{H}$ to trace the radiative intensity transferring in the n-layer composite, all of the RTCs can be obtained, and for simplicity, they are not written out here.

3.3. RTCs of an n-layer composite for absorbing–scattering sub-process

For an isotropically scattering composite, the scattered energy is equivalent to that emitted by the element (surface or control volume), and this property lets us could further apply the conception of RTCs, $(S_uS_v)^s_{k,o-o}$ etc., to trace the scattered energy, and finally deduce the RTCs of scattering medium, $[V_iV_j]^s_{k,o-o}$ etc. For simplicity, the detailed deductive processes are not written out here, and readers can get information from Refs. [20–22].

After the nth-order scattering event there are

$$[V_iS_u] = 4\alpha_b\Delta x_b[V_iS_u]^{*n\text{th}}_a, \qquad [V_iV_j] = 4\alpha_b\Delta x_b[V_iV_j]^{*n\text{th}}_a$$
$$[S_uS_v] = \varepsilon_u[S_uS_v]^{*n\text{th}}_a \quad \text{and} \quad [S_uV_j] = \varepsilon_u[S_uV_j]^{*n\text{th}}_a$$

where

$$\begin{aligned}[V_iS_u]^{*n\text{th}}_a &= [V_iS_u]^{*(n-1)\text{th}}_a + \sum_{l_2=1}^{M_t}(V_iV_{l_2})^*\omega'_{l_2} \\ &\quad\times\left\{\sum_{l_3=1}^{M_t}(V_{l_2}V_{l_3})^*\omega'_{l_3}\left\{\sum_{l_4=1}^{M_t}(V_{l_3}V_{l_4})^*\omega'_{l_4}\right.\right. \\ &\quad\bullet\cdots\bullet\left\{\sum_{l_{n-1}=1}^{M_t}(V_{l_{n-2}}V_{l_{n-1}})^*\omega'_{l_{n-1}}\right. \\ &\quad\left.\left.\left.\times\left[\sum_{l_n=1}^{M_t}(V_{l_{n-1}}V_{l_n})^*\omega'_{l_n}(V_{l_n}S_u)^*\right]\right\}\right\}\right\}\end{aligned} \tag{10}$$

$$\begin{aligned}[V_iV_j]^{*n\text{th}}_a &= [V_iV_j]^{*(n-1)\text{th}}_a + \sum_{l_2=1}^{M_t}(V_iV_{l_2})^*\omega'_{l_2} \\ &\quad\times\left\{\sum_{l_3=1}^{M_t}(V_{l_2}V_{l_3})^*\omega'_{l_3}\left\{\sum_{l_4=1}^{M_t}(V_{l_3}V_{l_4})^*\omega'_{l_4}\right.\right. \\ &\quad\bullet\cdots\bullet\left\{\sum_{l_{n-1}=1}^{M_t}(V_{l_{n-2}}V_{l_{n-1}})^*\omega'_{l_{n-1}}\right. \\ &\quad\left.\left.\left.\times\left[\sum_{l_n=1}^{M_t}(V_{l_{n-1}}V_{l_n})^*\omega'_{l_n}(V_{l_n}V_j)^*\eta'_j\right]\right\}\right\}\right\}\end{aligned} \tag{11}$$

$$\begin{aligned}[S_uS_v]^{*n\text{th}}_a &= [S_uS_v]^{*(n-1)\text{th}}_a + \sum_{l_2=1}^{M_t}(S_uV_{l_2})^*\omega'_{l_2} \\ &\quad\times\left\{\sum_{l_3=1}^{M_t}(V_{l_2}V_{l_3})^*\omega'_{l_3}\left\{\sum_{l_4=1}^{M_t}(V_{l_3}V_{l_4})^*\omega'_{l_4}\right.\right. \\ &\quad\bullet\cdots\bullet\left\{\sum_{l_{n-1}=1}^{M_t}(V_{l_{n-2}}V_{l_{n-1}})^*\omega'_{l_{n-1}}\right. \\ &\quad\left.\left.\left.\times\left[\sum_{l_n=1}^{M_t}(V_{l_{n-1}}V_{l_n})^*\omega'_{l_n}(V_{l_n}S_v)^*\right]\right\}\right\}\right\}\end{aligned} \tag{12}$$

$$\begin{aligned}[S_uV_j]^{*n\text{th}}_a &= [S_uV_j]^{*(n-1)\text{th}}_a + \sum_{l_2=1}^{M_t}(S_uV_{l_2})^*\omega'_{l_2} \\ &\quad\times\left\{\sum_{l_3=1}^{M_t}(V_{l_2}V_{l_3})^*\omega'_{l_3}\left\{\sum_{l_4=1}^{M_t}(V_{l_3}V_{l_4})^*\omega'_{l_4}\right.\right. \\ &\quad\bullet\cdots\bullet\left\{\sum_{l_{n-1}=1}^{M_t}(V_{l_{n-2}}V_{l_{n-1}})^*\omega'_{l_{n-1}}\right. \\ &\quad\left.\left.\left.\times\left[\sum_{l_n=1}^{M_t}(V_{l_{n-1}}V_{l_n})^*\omega'_{l_n}(V_{l_n}V_j)^*\eta'_j\right]\right\}\right\}\right\}\end{aligned} \tag{13}$$

3.4. Numerical method and flow chart of the calculation procedure

When solving Eq. (1) the radiative heat source term Φ^r_i should be linearized by Patankar's method at first [3]:

$$\begin{aligned}\Phi^{r,m,n+1}_i &= \Phi^{r,m,n}_i + \left(\mathrm{d}\Phi^r_i/\mathrm{d}T_i\right)^{m,n}\left(T^{m,n+1}_i - T^{m,n}_i\right) \\ &= Sc^{m,n+1}_i + Sp^{m,n+1}_i T^{m,n+1}_i\end{aligned} \tag{14}$$

where superscripts n and $n+1$ denote the nth and $(n+1)$th iterative calculations; Sp_i ($\leqslant 0$) is the modulus of T_i; Sc_i represents the constant part of Φ^r_i. Solving the linearized equations by the tri-diagonal matrix algorithm (TDMA) gives the temperatures of all nodes. The flow charts of the procedure for calculating the temperature field and the RTCs are presented in Appendix C.

Table 1
Comparison of results of this paper with those of Ref. [7] and Ref. [22] for transient case

References compared with	Dimensionless temperature, T/T_r			Dimensionless radiative heat flux, $q/(k_1\kappa_1 T_r)$		
	$X=1/4$	$X=1/2$	$X=3/4$	$X=0$	$X=1/2$	$X=1$
Ref. [7]: Eighth-order approximation	0.4893	0.1773	0.0587	1.9342	1.3289	0.8319
Ref. [22]: $\Delta t^* = t^*_{\text{Ref. [7]}}/5000,\ M_t = 200$	0.48935	0.17731	0.05869	1.93422	1.32883	0.83190
This paper	0.48924	0.17729	0.05871	1.93425	1.32880	0.83188

3.5. Validation of this paper

A 30-point Gauss quadrature scheme is used to integrate the RTC expressions, such as Eq. (9), and the precision of Gauss quadrature is chosen as 10^{-6}. The correctness is validated from the following two aspects.

First the correctness of spectral RTCs has been validated by Eq. (5) and the following equation in all the following calculations:

$$\sum_{j=1}^{M_t}[V_iV_j]^s_{k,o-o} + [V_iS_1]^s_{k,o-o} + [V_iS_2]^s_{k,o-o} = 4\kappa_{b,k}\Delta x_b \quad V_i \in b\text{th layer} \tag{15a}$$

$$[S_1S_1]^s_{k,o-o} + \sum_{j=1}^{M_t}[S_1V_j]^s_{k,o-o} + [S_1S_2]^s_{k,o-o} = \varepsilon_{1,k} \tag{15b}$$

$$[S_2S_1]^s_{k,o-o} + \sum_{j=1}^{M_t}[S_2V_j]^s_{k,o-o} + [S_2S_2]^s_{k,o-o} = \varepsilon_{2,k} \tag{15c}$$

Second the comparison of the results of this paper with those of Ref. [7] and Ref. [22], which investigated the transient coupled heat transfer in a single absorbing, isotropically scattering layer with black opaque surfaces, shows good agreement, as shown in Table 1. The parameters are $n = 1, n_1 = 1$,

$\varepsilon_1 = \varepsilon_2 = 1, \quad L_1\kappa_1 = 1, \quad T_{S_1} = T_r = 1000$ K

$T_{S_2} = T_0 = 0$ K, $\quad \omega_1 = 0.5$

$t^*_{\text{Ref. [7]}} = k_1\kappa^2 t/(\rho_1 c_1) = 0.05$ (defined by Ref. [7]) and $N_{1,\text{Ref. [7]}} = k_1\kappa_1/(4\sigma T_r^3) = 0.1$. The control volumes and dimensionless constant time step are $M_1 = 350$ and $\Delta t^* = t^*_{\text{Ref. [7]}}/1000$.

4. Results and discussions

In all the following calculations, the constant dimensionless time step, $\Delta t^* = t^*/1000$, is applied, and steady state is defined to be reached if $|T_i^{m+1} - T_i^m| < 10^{-5}$.

4.1. Effect of refractive index on transient coupled heat transfer

From Figs. 3–5, transient coupled heat transfer in a four-layer gray composite is studied, and in all the three figures

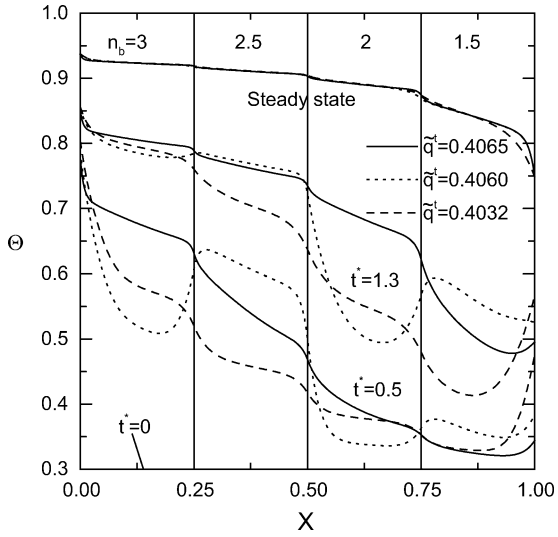

Fig. 3. Effect of arranging refractive indexes decreasing along the thickness on transient coupled heat transfer

the solid lines are for $\omega_1 = \omega_2 = \omega_3 = \omega_4 = 0$, the dotted lines are for $\omega_1 = \omega_3 = 0.9, \omega_2 = \omega_4 = 0$, the dashed lines are for $\omega_1 = \omega_2 = \omega_3 = \omega_4 = 0.9$, and the control volume of each layer is chosen as $M_b = 100$.

In Fig. 3, the refractive indexes are arranged decreasing along the whole thickness of composite. Except for the scattering albedo, the other parameters for the three-sort curves are the same:

$\varepsilon_0 = \varepsilon_1 = \varepsilon_2 = \varepsilon_3 = 0.8, \quad T_{-\infty} = T_{g1} = T_r = 1000$ K

$T_{+\infty} = T_{g2} = T_0 = 300$ K, $\quad h_1 = 200$ W·m^2·K^{-1}

$h_2 = 20$ W·m^2·K^{-1}, $\quad \rho_b c_b =$ constant $\quad (b = 1$ to $4)$

$N_b = 0.002, \quad L_b = 0.008$ m and $\kappa_b = 100$ m^{-1}

As shown in Fig. 3, the heating of $S_{-\infty}$ and the left surrounding fluid causes the temperature of S_1 to rise quickly. Then the inside of S_1 emits radiative energy to the inner part of the composite and causes the temperatures therein to increase. If there is no scattering, as shown in solid lines, the temperature distribution decreases gradually in the most part of the composite, but concaves upward near S_2 because the inside of S_2 absorbs more radiative energy than its near medium does. The reflection of interface causes the temperature curves at interface to be bended intensively. When the first and the third layers are scattering (dotted lines), most of the radiative energy that reaches them is scattered. This causes much more radiative energy to be

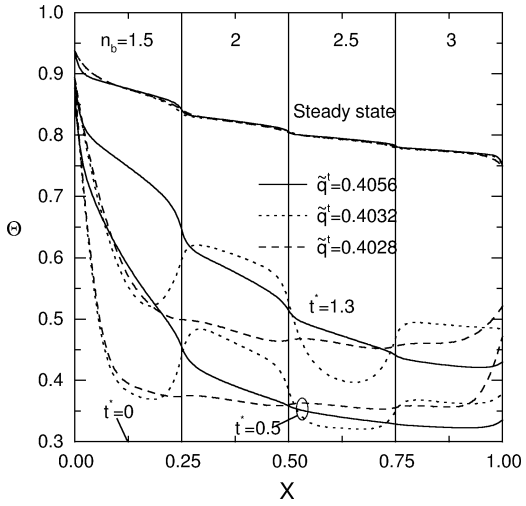

Fig. 4. Effect of arranging refractive indexes increasing along the thickness on transient coupled heat transfer.

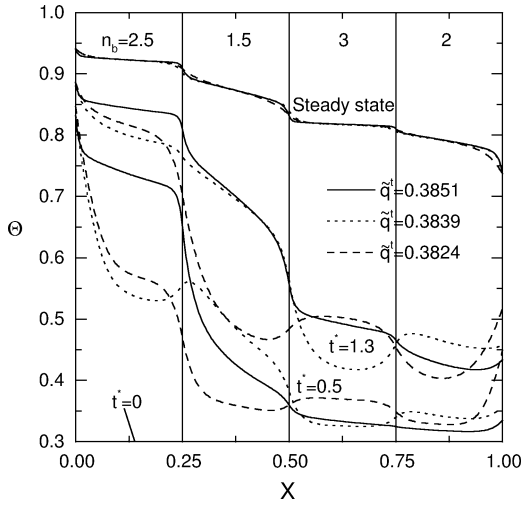

Fig. 5. Effect of arranging refractive indexes arbitrarily on transient coupled heat transfer.

absorbed by the second and the fourth layers and S_2, so as shown by dotted lines, during the transient process, two maximum temperature peaks appear in the second and the fourth layers and the temperature of S_2 is higher than that of solid line. When all the four layers scatter isotropically, as shown by dashed lines, in the beginning of this transient process, the temperature of S_2 is much higher than that of solid lines and dotted lines because the intensified scattering causes more radiative energy to be absorbed by S_2. At steady state, the three curves are very close, so isotropic scattering causes less effect on steady state than it does on transient course. As indicated in Fig. 3, the more intensively the composite scatters, the smaller the steady heat flux is. So, although the total optical thickness of the composite is unchanged, the scattering increases the resistance of the composite to the transferring of radiative energy.

In Fig. 4, the refractive indexes are arranged increasing along the thickness. Except for the refractive index arrangement, the other parameters of this figure are the same as those of Fig. 3. Compared with Fig. 3, the decrease in the refractive index of the first layer causes the emitting ability inside of S_1 to be weakened seriously because the emitting ability of medium is in proportion to the square of refractive index, and the energy that S_1 absorbs from $S_{-\infty}$ and the surrounding fluid cannot be adequately reemitted to the inner part of the composite. So the temperature of S_1 is higher than that of Fig. 3, the temperature of most part of the composite rises slowly, and the steady heat flux is smaller than that of corresponding curve in Fig. 3.

In Fig. 5, the refractive indexes are arranged arbitrary, so the total reflection phenomenon becomes more complex than that in Figs. 3 and 4. The steady heat flux is smaller than that of corresponding curve in Figs. 3 and 4, respectively. The reason mainly relates to the emitting inside of S_1 and reflection and total reflection at all interfaces. In this figure, $n_1(= 2.5)$ is bigger than that in Fig. 4, and this makes the total reflection at the left sides of all the interfaces to be enhanced, while the emitting ability inside of S_1 is strengthened. The intensified reflection causes the resistance of the radiative energy's transferring from left to right to be increased, and this increased resistance takes more effects on decreasing steady heat flux than the strengthened emitting ability inside of S_1 does on increasing steady heat flux. However, in Fig. 3, where $n_1 = 3$, the intensified emitting ability inside of S_1 plays a more important role on increasing steady heat flux than the intensified reflection and total reflection at the left sides of all the interfaces does on decreasing steady heat flux. As shown in dashed lines, in the beginning of the transient process, a maximum temperature peak appears in the third layer. This is mainly caused by total reflection, which is due to the third layer's biggest refractive index and having critical angles to all the other layers. When the incident angle of scattered energy is greater than critical angle of interface, the scattered energy is totally reflected back. This total reflection phenomenon to scattered energy makes the third layer absorbs more radiative energy than its neighboring media, then a maximum temperature peak appears therein.

In Figs. 6(a) and (b), the layer number increases to 16, the refractive indexes are arranged more continuous than that in Figs. 3 and 4, respectively. The thickness and extinction coefficient of each layer are $L_b = 0.002$ m and $\kappa_b = 100\ \mathrm{m}^{-1}$, so the total thickness and total optical thickness of the composite of the two figures are the same as those of Figs. 3 and 4. The number of control volume in each layer is $M_b = 25$. The solid lines are for $\omega_b = 0$ ($b = 1$ to 16), the dotted lines are for $\omega_{b=2i-1} = 0.9$ and $\omega_{b=2i} = 0.0$, where $i = 1$ to 8, and the dashed lines are for $\omega_b = 0.9$ ($b = 1$ to 16). Except the arrangement of refractive index, the other parameters of the two figures are the same as those of Fig. 3. When the decrement (Fig. 6(a)) or the increment (Fig. 6(b)) of refractive index becomes small, the reflection and total reflection is weakened at all the interfaces, and this coupled with the conduction makes the temperature profiles in the

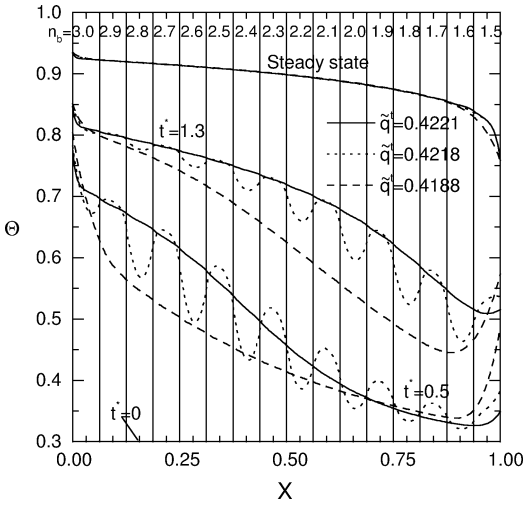

(a)

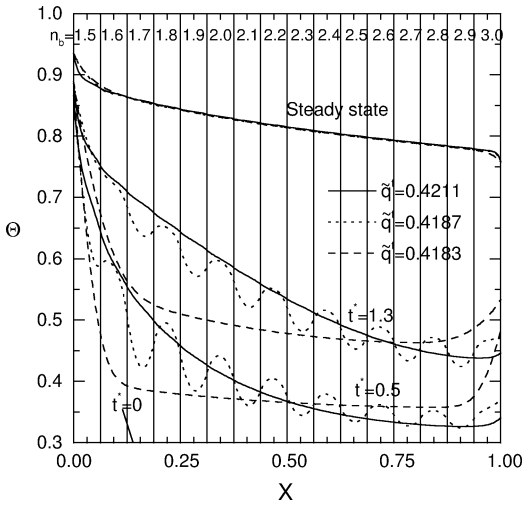

(b)

Fig. 6. Effect of uniform refractive index change on transient coupled heat transfer: (a) arranging refractive index decreasing along the thickness; (b) arranging refractive index increasing along the thickness.

composite become very smooth. When odd layers scatter but even layers do not, as shown in dotted lines in the two figures, in the beginning of the transient process, the temperature profile resembles a sine wave. Also the more intensively the composite scatters, the smaller the steady heat flux is, and the steady heat flux in Fig. 6(a) is greater than that of corresponding curve in Fig. 6(b), so arranging refractive index decreasing is of advantage for increasing steady heat flux. Compared with Figs. 3 and 4, respectively, the steady heat flux of corresponding curve in the two figures increases a lot.

4.2. Effect of vacuum space on transient coupled heat transfer

The multi-layer model also can calculate the special case that several layers are separated by vacuum spaces, because vacuum space can be treated as a special layer that does not conduct, does not attenuate radiative energy and has a unit refractive index. So in the following calculations, the conduction-radiation parameter, the volume specific heat capacity, and the optical thickness of the vacuum space layer are chosen very small, such as $N_{va} = 10^{-100}$, $\rho_{va}c_{va} = 10^{-100}$ J·m^{-3}·K^{-1}, and $\kappa_{va}L_{va} = 10^{-9}$ with thickness $L_{va} = 10^{-11}$ m, and refractive index $n_{va} = 1$. And the whole vacuum space layer is treated as one control volume.

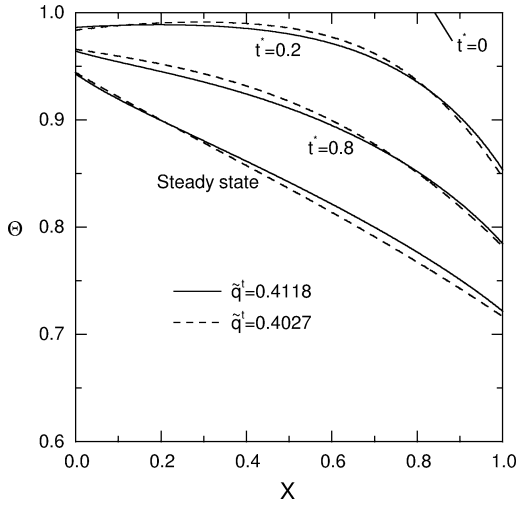

Fig. 7. Transient coupled heat transfer in a single layer.

In Fig. 7, the transient coupled heat transfer in a one-layer medium with three spectral bands ($NB = 3$) properties of $\kappa_{1,k} = 20,\ 400,\ 10\,000$ m^{-1} corresponding to $\lambda = 0 \sim 2.7,\ 2.7 \sim 4.4,\ 4.4 \sim \infty$ μm, and $n_{1,k} = 1.5$, which are similar to glass[8], is investigated. The surrounding parameters are the same as those in Section 4.1: $T_{-\infty} = T_{g1} = 1000$ K, $T_{+\infty} = T_{g2} = 300$ K, $h_1 = 200$ W·m^{-2} K^{-1}, and $h_2 = 20$ W·m^{-2}·K^{-1}. The other parameters are $L_1 = 0.03$ m, $N_1 = 0.18$, $T_0 = T_r = 1000$ K, $\varepsilon_0 = \varepsilon_3 = 1.0$ and $\varepsilon_1 = \varepsilon_2 = 0.8$. The control volume is $M_1 = 600$. And from Figs. 7 to 9, the solid lines are for $\omega_{b,k} = 0$, and the dashed lines are for $\omega_{b,k} = 0.9$. As shown in Fig. 7, isotropic scattering causes the steady heat flux to decrease for the medium with spectral properties.

Then, the single layer of Fig. 7 is divided into two equal parts that are separated by one vacuum space.

The thickness and the control volume of each layer become $L_b = 0.015$ m and $M_b = 300$. The interfaces between the two layers and vacuum space are semitransparent and specular, so the two layers only exchange radiative energy with each other through the vacuum space. For this condition, by using a three-layer model ($n = 3$) with the second layer to be a vacuum space layer, the transient coupled heat transfer problem can be studied. The results are illustrated in Fig. 8, in which the surrounding parameters, the initial and reference temperatures and the spectral properties of the semitransparent layer are completely the same with those of Fig. 7.

As shown in Fig. 8, the temperature of the right layer is much higher than that of the left layer because the

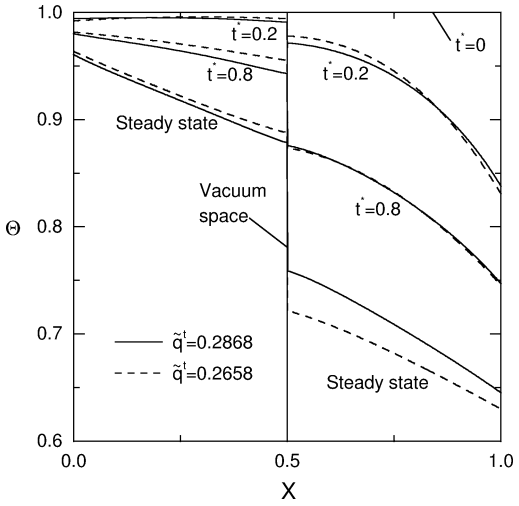

Fig. 8. Effect of one vacuum space on transient coupled heat transfer.

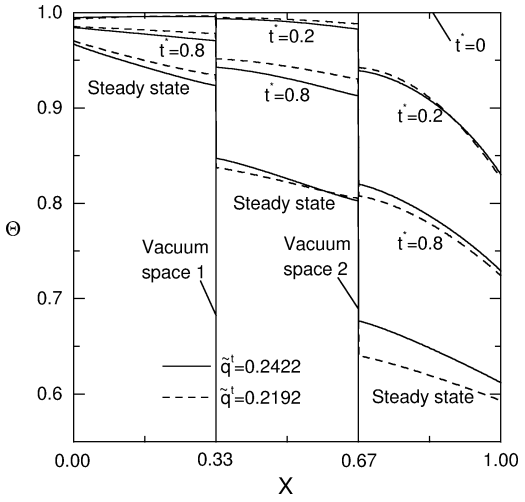

Fig. 9. Effect of two vacuum spaces on transient coupled heat transfer.

reflection, especially total reflection, at the interface between the left layer and the vacuum space intensively resists the transferring of radiative energy from left to right. There is temperature difference between the two interfaces that are separated by vacuum space. At steady state the temperature of the right layer indicated by dashed line is obviously lower than that indicated by solid line, so this illustrates that the resistance of vacuum space for scattering condition is greater than that for non-scattering condition, and as shown in the figure, the steady heat flux of dashed line decreases. Compared with Fig. 7, the vacuum space causes the steady state heat flux to decrease greatly.

Fig. 9 illustrates the transient coupled heat transfer process for the condition that the single layer of Fig. 7 is divided into three equal parts, which are separated one another by two vacuum spaces. The interfaces between the layers and the vacuum spaces are semitransparent and specular. Except for thickness ($L_b = 0.01$ m) and control volume number ($M_b = 200$) of each layer, the other parameters of this figure are the same with those of Fig. 7. The temperature difference between the interfaces separated by vacuum space 2 is larger than that between the interfaces separated by vacuum space 1. The transient temperature of the left layer is very high and changes slowly with time, that of the right layer is very low and changes quickly with time, and that of the central layer does moderately. The isotropic scattering hinders the radiative transfer, and the steady heat flux decreases. Compared with Fig. 8, the steady heat flux of corresponding curve decreases. So the increase in vacuum space number causes the resistance to heat flux to increase, and the steady heat flux decreases.

5. Conclusion

By using the ray tracing method, combined with the spectral band model and Hottel and Sarofim's zonal method, the RTCs for a multi-layer absorbing, emitting, and isotropic scattering composite are derived. The boundaries of the composite are opaque and specular, and the interfaces of the composite are semitransparent and specular. Resorting to RTCs, the radiative heat source term is calculated. The transient energy equation is solved by the fully implicit discrete control-volume method.

By using the multi-layer composite model, the effects of refractive index and vacuum space on transient coupled radiative and conductive heat transfer are investigated. The following conclusions are obtained:

(1) Keeping extinction coefficient unchanged, the isotropic scattering decreases the steady heat flux. The more intensively the composite scatters, the smaller the steady heat flux is.
(2) From high temperature surrounding side to the low one, arranging refractive indexes decreasing along the thickness can cause larger steady heat flux than arranging refractive indexes increasing.
(3) If the decrement or the increment of refractive index along the thickness decreases as the layer number increases, the temperature profile becomes smooth and the steady heat flux increases.
(4) Isotropic scattering increases the resistance of vacuum space to radiation, and the steady heat flux decreases.
(5) The more the vacuum spaces are, the smaller the steady heat flux is.

Acknowledgements

This research is supported by the Chinese National Science Fund for Distinguished Young Scholars (No. 59725617) and Doctorial Subject Special Fund of High School of Ministry of Education of China.

Appendix A. One-layer radiative intensity quotient transfer functions

The function that describes the radiative intensity transfer law in a single semitransparent layer is defined as one-layer radiative intensity quotient transfer function, which is represented by symbol $\boldsymbol{F}_{a1_b,k}^{a2_b}$. Symbol $\boldsymbol{F}_{a1_b,k}^{a2_b}$ means the ratios of the spectral radiative intensity arriving at superscript $a2_b$ to that emitted by subscript $a1_b$ at kth spectral band. Because the formulation form and the deducing process are the same no matter the medium is gray or non-gray, the subscript k is omitted below.

As shown in Fig. A.1, P_{b-1} and P_b are the two boundaries of bth layer. When the radiative intensity, emitted by the mth element (surface or control volume) at θ direction, enters the bth layer through P_{b-1} or P_b, it will be reflected and attenuated repeatedly within the layer until it finally becomes 0. By tracing this transfer process, the following expressions of the radiative intensity quotient transfer function are obtained.

$$\begin{aligned}\boldsymbol{F}_{P_{b-1'}}^{V_{I_b}} &= \big\{\rho(\theta)_{b,b+1}\exp\big[-\kappa_b\big(L_b + x_{(I+1)_b}^{P_b}\big)/\mu_b\big] \\ &\quad + \exp\big(-\kappa_b x_{I_b}^{P_{b-1'}}/\mu_b\big)\big\} \\ &\quad \times\big[1-\exp(-\kappa_b\Delta x_b/\mu_b)\big]/(1-\beta_1) \qquad \text{(A.1a)}\\ \boldsymbol{F}_{P_b}^{V_{I_b}} &= \big\{\rho(\theta)_{b,b-1}\exp\big[-\kappa_b\big(L_b + x_{I_b}^{P_{b-1'}}\big)/\mu_b\big] \\ &\quad + \exp\big(-\kappa_b x_{(I+1)_b}^{P_b}/\mu_b\big)\big\} \\ &\quad \times\big[1-\exp(-\kappa_b\Delta x_b/\mu_b)\big]/(1-\beta_1) \qquad \text{(A.1b)}\end{aligned}$$

$$\boldsymbol{F}_{P_b}^{P_b} = \exp(-2\kappa_b L_b/\mu_b)\rho(\theta)_{b,b-1}/(1-\beta_1) \qquad \text{(A.1c)}$$

$$\boldsymbol{F}_{P_{b-1'}}^{P_{b-1'}} = \exp(-2\kappa_b L_b/\mu_b)\rho(\theta)_{b,b+1}/(1-\beta_1) \qquad \text{(A.1d)}$$

$$\boldsymbol{F}_{P_{b-1'}}^{P_b} = \boldsymbol{F}_{P_b}^{P_{b-1'}} = \exp(-\kappa_b L_b/\mu_b)/(1-\beta_1) \qquad \text{(A.1e)}$$

$$\beta_1 = \exp(-2\kappa_b L_b/\mu_b)\rho(\theta)_{b,b-1}\rho(\theta)_{b,b+1} \qquad \text{(A.1f)}$$

where $x_{(I+1)_b}^{P_b} = L_b - I\Delta x_b$, $x_{I_b}^{P_{b-1}} = (I-1)\Delta x_b$, and Δx_b is the control volume thickness of the bth layer, and $\mu_b = \cos\theta_b$, where θ_b is the refractive angle of the bth layer. According to the Snell refractive law,

$$\theta_b = \arcsin(\sin\theta\cdot n_m/n_b) \qquad \text{(A.2)}$$

where n_m is the refractive index of the mth element.

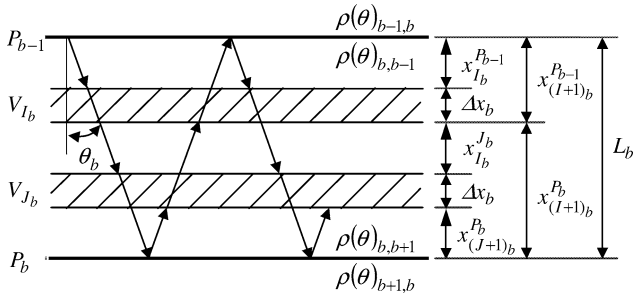

Fig. A.1. Radiative intensity transfer model one-layer semitransparent medium.

The radiative intensity emitted by the Ith control volume V_{I_b} is still reflected and attenuated repeatedly within the layer until it finally becomes 0. By tracing this process, the following expressions of the radiative intensity quotient transfer function are obtained.

$$\boldsymbol{F}_{V_{I_b}}^{P_b} = \boldsymbol{F}_{P_b}^{V_{I_b}} \qquad \text{(A.3a)}$$

$$\boldsymbol{F}_{V_{I_b}}^{P_{b-1'}} = \boldsymbol{F}_{P_{b-1'}}^{V_{I_b}} \qquad \text{(A.3b)}$$

$$\begin{aligned}\boldsymbol{F}_{V_{I_b}}^{V_{I_b}} &= \big\{\rho(\theta)_{b,b-1}\exp\big(-2\kappa_b x_{I_b}^{P_{b-1'}}/\mu_b\big) \\ &\quad + \rho(\theta)_{b,b+1}\exp\big(-2\kappa_b x_{(I+1)_b}^{P_b}/\mu_b\big) \\ &\quad + 2\rho(\theta)_{b,b-1}\rho(\theta)_{b,b+1} \\ &\quad \times\exp\big[-\kappa_b\big(x_{I_b}^{P_{b-1'}} + L_b + x_{(I+1)_b}^{P_b}\big)/\mu_b\big]\big\} \\ &\quad \times\big[1-\exp(-\kappa_b\Delta x_b/\mu_b)\big]^2/(1-\beta_1) \qquad \text{(A.3c)}\\ \boldsymbol{F}_{V_{I_b}}^{V_{J_b}} &= \big\{\exp\big(-\kappa_b x_{I_b}^{J_b}/\mu_b\big) \\ &\quad + \rho(\theta)_{b,b-1}\exp\big[-\kappa_b\big(x_{I_b}^{P_{b-1'}} + x_{J_b}^{P_{b-1'}}\big)/\mu_b\big] \\ &\quad + \rho(\theta)_{b,b+1}\exp\big[-\kappa_b\big(x_{(I+1)_b}^{P_b} + x_{(J+1)_b}^{P_b}\big)/\mu_b\big] \\ &\quad + \rho(\theta)_{b,b-1}\rho(\theta)_{b,b+1} \\ &\quad \times\exp\big[-\kappa_b\big(2L_b - 2\Delta x_b - x_{V_{I_b}}^{V_{J_b}}\big)/\mu_b\big]\big\} \\ &\quad \times\big[1-\exp(-\kappa_b\Delta x_b/\mu_b)\big]^2/(1-\beta_1) \qquad \text{(A.3d)}\end{aligned}$$

where $x_{I_b}^{J_b} = (|I-J|-1)\Delta x_b$, which is the distance between control volumes V_{I_b} and V_{J_b}, as shown in Fig. A.1.

In Eq. (A.3d), $\boldsymbol{F}_{V_{I_b}}^{V_{I_b}}$ denotes the quotient of the radiative intensity finally attenuated by V_{I_b} to that emitted by V_{I_b} after it passes through the boundaries I_b and $(I+1)_b$ of the control volume and transfers in the layer. But before the radiative energy, emitted by V_{I_b}, passes through the boundaries I_b and $(I+1)_b$, part of it that has been attenuated by the control volume itself can be expressed as $4\kappa_b\Delta x_b - 2[1-2E_3(\kappa_b\Delta x_b)]$. That is, it is necessary to add this term when calculating the RTC $(V_{I_b}V_{I_b})_{o-o,k}^{s}$.

Furthermore P_0 and P_n will appear in Eqs. (A.1) and (A.3) when calculating the first and the nth layer, and they need to be replaced by S_1 and S_2, respectively.

Appendix B. Deduction of radiative heat source term

In Eq. (1), the effect of radiation on transient coupled heat transfer is considered as a radiative source term, Φ_i^r, which can be calculated from the expression, $\Phi_i^r = q_{iw}^r - q_{ie}^r = q_{iw}^r - q_{(i+1)w}^r$. Where, q_{iw}^r represents the net radiative energy passing through the left boundary of control volume i, and $q_{ie}^r = q_{(i+1)w}^r$ represents that passing through the right boundary of control volume i. By using RTCs q_{iw}^r can be expressed as

$$
\begin{aligned}
q_{iw}^r = \sigma \sum_{k=1}^{NB} \Bigg\{ & \sum_{j=i}^{M_t} \Big[n_{1,k}'^2 [S_1 V_j]_{k,o-o}^s A_{k,T_{S_1}} T_{S_1}^4 \\
& - n_{j,k}'^2 [V_j S_1]_{k,o-o}^s A_{k,T_j} T_j^4 \Big] \\
& + \sum_{l=1}^{i-1} \sum_{j=i}^{M_t} \Big[n_{l,k}'^2 [V_l V_j]_{k,o-o}^s A_{k,T_l} T_l^4 \\
& - n_{j,k}'^2 [V_j V_l]_{k,o-o}^s A_{k,T_j} T_j^4 \Big] \\
& + \sum_{l=1}^{i-1} \Big[n_{l,k}'^2 [V_l S_2]_{k,o-o}^s A_{k,T_l} T_l^4 \\
& - n_{M_t,k}'^2 [S_2 V_l]_{k,o-o}^s A_{k,T_{S_2}} T_{S_2}^4 \Big] \\
& + \Big[n_{1,k}'^2 [S_1 S_2]_{k,o-o}^s A_{k,T_{S_1}} T_{S_1}^4 \\
& - n_{M_t,k}'^2 [S_2 S_1]_{k,o-o}^s A_{k,T_{S_2}} T_{S_2}^4 \Big] \Bigg\}
\end{aligned} \tag{B.1}
$$

Similarly $q_{ie}^r (= q_{(i+1)w}^r)$ can be expressed as

$$
\begin{aligned}
q_{ie}^r = \sigma \sum_{k=1}^{NB} \Bigg\{ & \sum_{j=i+1}^{M_t} \Big[n_{1,k}'^2 [S_1 V_j]_{k,o-o}^s A_{k,T_{S_1}} T_{S_1}^4 \\
& - n_{j,k}'^2 [V_j S_1]_{k,o-o}^s A_{k,T_j} T_j^4 \Big] \\
& + \sum_{l=1}^{i} \sum_{j=i+1}^{M_t} \Big[n_{l,k}'^2 [V_l V_j]_{k,o-o}^s A_{k,T_l} T_l^4 \\
& - n_{j,k}'^2 [V_j V_l]_{k,o-o}^s A_{k,T_j} T_j^4 \Big] \\
& + \sum_{l=1}^{i} \Big[n_{l,k}'^2 [V_l S_2]_{k,o-o}^s A_{k,T_l} T_l^4 \\
& - n_{M_t,k}'^2 [S_2 V_l]_{k,o-o}^s A_{k,T_{S_2}} T_{S_2}^4 \Big] \\
& + \Big[n_{1,k}'^2 [S_1 S_2]_{k,o-o}^s A_{k,T_{S_1}} T_{S_1}^4 \\
& - n_{M_t,k}'^2 [S_2 S_1]_{k,o-o}^s A_{k,T_{S_2}} T_{S_2}^4 \Big] \Bigg\}
\end{aligned} \tag{B.2}
$$

Subject Eqs. (B.1) and (B.2) to a transformation as follows:

$$
\begin{aligned}
q_{iw}^r = \sigma \sum_{k=1}^{NB} \Bigg\{ & \sum_{j=i+1}^{M_t} \Big[n_{1,k}'^2 [S_1 V_j]_{k,o-o}^s A_{k,T_{S_1}} T_{S_1}^4 \\
& - n_{j,k}'^2 [V_j S_1]_{k,o-o}^s A_{k,T_j} T_j^4 \Big] \\
& + \Big[n_{1,k}'^2 [S_1 V_i]_{k,o-o}^s A_{k,T_{S_1}} T_{S_1}^4 \\
& - n_{i,k}'^2 [V_i S_1]_{k,o-o}^s A_{k,T_i} T_i^4 \Big] \\
& + \sum_{l=1}^{i-1} \sum_{j=i+1}^{M_t} \Big[n_{l,k}'^2 [V_l V_j]_{k,o-o}^s A_{k,T_l} T_l^4 \\
& - n_{j,k}'^2 [V_j V_l]_{k,o-o}^s A_{k,T_j} T_j^4 \Big] \\
& + \sum_{l=1}^{i-1} \Big[n_{l,k}'^2 [V_l V_i]_{k,o-o}^s A_{k,T_l} T_l^4 \\
& - n_{i,k}'^2 [V_i V_l]_{k,o-o}^s A_{k,T_i} T_i^4 \Big] \\
& + \sum_{l=1}^{i-1} \Big[n_{l,k}'^2 [V_l S_2]_{k,o-o}^s A_{k,T_l} T_l^4 \\
& - n_{M_t,k}'^2 [S_2 V_l]_{k,o-o}^s A_{k,T_{S_2}} T_{S_2}^4 \Big] \\
& + \Big[n_{1,k}'^2 [S_1 S_2]_{k,o-o}^s A_{k,T_{S_1}} T_{S_1}^4 \\
& - n_{M_t,k}'^2 [S_2 S_1]_{k,o-o}^s A_{k,T_{S_2}} T_{S_2}^4 \Big] \Bigg\}
\end{aligned} \tag{B.3}
$$

$$
\begin{aligned}
q_{ie}^r = \sigma \sum_{k=1}^{NB} \Bigg\{ & \sum_{j=i+1}^{M_t} \Big[n_{1,k}'^2 [S_1 V_j]_{k,o-o}^s A_{k,T_{S_1}} T_{S_1}^4 \\
& - n_{j,k}'^2 [V_j S_1]_{k,o-o}^s A_{k,T_j} T_j^4 \Big] \\
& + \sum_{l=1}^{i-1} \sum_{j=i+1}^{M_t} \Big[n_{l,k}'^2 [V_l V_j]_{k,o-o}^s A_{k,T_l} T_l^4 \\
& - n_{j,k}'^2 [V_j V_l]_{k,o-o}^s A_{k,T_j} T_j^4 \Big] \\
& + \sum_{j=i+1}^{M_t} \Big[n_{i,k}'^2 [V_i V_j]_{k,o-o}^s A_{k,T_i} T_i^4 \\
& - n_{j,k}'^2 [V_j V_i]_{k,o-o}^s A_{k,T_j} T_j^4 \Big] \\
& + \sum_{l=1}^{i-1} \Big[n_{l,k}'^2 [V_l S_2]_{k,o-o}^s A_{k,T_l} T_l^4 \\
& - n_{M_t,k}'^2 [S_2 V_l]_{k,o-o}^s A_{k,T_{S_2}} T_{S_2}^4 \Big] \\
& + \Big[n_{i,k}'^2 [V_i S_2]_{k,o-o}^s A_{k,T_i} T_i^4 \\
& - n_{M_t,k}'^2 [S_2 V_i]_{k,o-o}^s A_{k,T_{S_2}} T_{S_2}^4 \Big] \\
& + \Big[n_{1,k}'^2 [S_1 S_2]_{k,o-o}^s A_{k,T_{S_1}} T_{S_1}^4 \\
& - n_{M_t,k}'^2 [S_2 S_1]_{k,o-o}^s A_{k,T_{S_2}} T_{S_2}^4 \Big] \Bigg\}
\end{aligned} \tag{B.4}
$$

Then from Eqs. (B.3) and (B.4), the radiative heat source term can be easily calculated:

$$
\begin{aligned}
\Phi_i^r &= q_{iw}^r - q_{ie}^r \\
&= \sigma \sum_{k=1}^{NB} \Bigg\{ n_{1,k}'^2 [S_1 V_i]_{k,o-o}^s A_{k,T_{S_1}} T_{S_1}^4 \\
&\quad - n_{i,k}'^2 [V_i S_1]_{k,o-o}^s A_{k,T_i} T_i^4 \\
&\quad + \sum_{l=1}^{i-1} \Big[n_{l,k}'^2 [V_l V_i]_{k,o-o}^s A_{k,T_l} T_l^4 \\
&\quad - n_{j,k}'^2 [V_i V_l]_{k,o-o}^s A_{k,T_i} T_i^4 \Big] \\
&\quad + \sum_{j=i+1}^{M_t} \Big[n_{j,k}'^2 [V_j V_i]_{k,o-o}^s A_{k,T_j} T_j^4 \\
&\quad - n_{l,k}'^2 [V_i V_j]_{k,o-o}^s A_{k,T_i} T_i^4 \Big] \\
&\quad + \Big[n_{M_t,k}'^2 [S_2 V_i]_{k,o-o}^s A_{k,T_{S_2}} T_{S_2}^4 \\
&\quad - n_{l,k}'^2 [V_i S_2]_{k,o-o}^s A_{k,T_i} T_i^4 \Big] \Bigg\}
\end{aligned} \tag{B.5}
$$

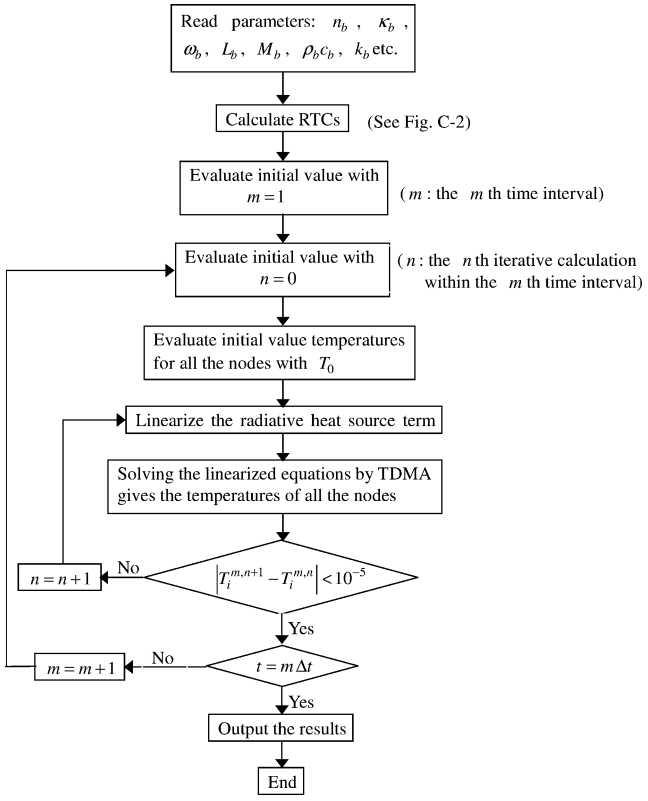

Fig. C.1. Flow chart of the procedure for calculating the temperature field.

and for simplicity Eq. (B.5) also can be expressed as

$$\begin{aligned}\Phi_i^r = \sigma \sum_{k=1}^{NB} \Bigg\{ & n_{1,k}'^2 [S_1 V_i]_{k,o-o}^s A_{k,T_{S_1}} T_{S_1}^4 \\ & - n_{i,k}'^2 [V_i S_1]_{k,o-o}^s A_{k,T_i} T_i^4 \\ & + \sum_{l=1}^{M_t} \Big[n_{l,k}'^2 [V_l V_i]_{k,o-o}^s A_{k,T_l} T_l^4 \\ & - n_{j,k}'^2 [V_i V_l]_{k,o-o}^s A_{k,T_i} T_i^4 \Big] \\ & + \Big[n_{M_t,k}'^2 [S_2 V_i]_{k,o-o}^s A_{k,T_{S_2}} T_{S_2}^4 \\ & - n_{i,k}'^2 [V_i S_2]_{k,o-o}^s A_{k,T_i} T_i^4 \Big] \Bigg\} \end{aligned} \quad \text{(B.6)}$$

Appendix C. Flow chart of the procedure

The flow chart of the procedure for calculating the temperature field is shown in Fig. C.1, and that of the procedure for calculating the RTCs is shown in Fig. C.2.

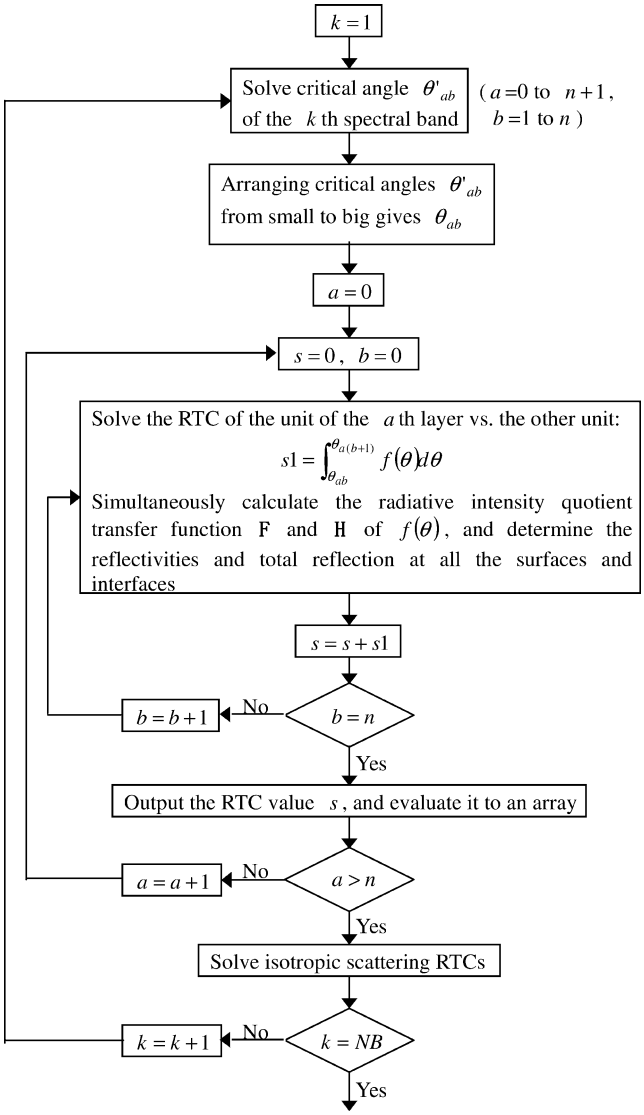

Fig. C.2. Flow chart of the procedure for calculating the RTCs.

References

[1] R. Siegel, Transient thermal analysis of a translucent thermal barrier coating on a metal wall, ASME J. Heat Transfer 121 (1999) 478–481.

[2] R. Siegel, Temperature distributions in channel walls with translucent thermal barrier coatings, AIAA J. Thermophys. Heat Transfer 12 (1998) 289–296.

[3] H.P. Tan, M. Lallemand, Transient radiative–conductive heat transfer in flat glasses submitted to temperature, flux and mixed boundary conditions, Internat. J. Heat Mass Transfer 32 (1989) 795–810.

[4] D. Schwander, G. Flamant, G. Olalde, Effects of boundary properties on transient temperature distributions in condensed semitransparent media, Internat. J. Heat Mass Transfer 33 (1990) 1685–1695.

[5] R.E. Field, R. Viskanta, Measurement and prediction of dynamic temperatures in unsymmetrically Cooled Glass Windows, AIAA J. Thermophys. Heat Transfer 7 (1993) 616–623.

[6] M.H. Su, W.H. Sutton, Transient conductive and radiative heat transfer in a silica window, AIAA J. Thermophys. Heat Transfer 9 (1995) 370–373.

[7] J.I. Frankel, Cumulative variable formulation for transient conductive and radiative transport in participating medium, AIAA J. Thermophys. Heat Transfer 9 (1995) 210–218.

[8] R. Siegel, C.M. Spuckler, Effects of refractive index and diffuse or specular boundaries on a radiating isothermal layer, ASME J. Heat Transfer 116 (1994) 787–790.

[9] R. Siegel, Transient heat transfer in a semitransparent radiation layer with boundary convection and surface reflection, Internat. J. Heat Mass Transfer 39 (1996) 69–79.

[10] U. Heinemann, R. Caps, J. Fricke, Radiation–conduction interaction: An investigation on silica aerogels, Internat. J. Heat Mass Transfer 39 (1996) 2115–2130.

[11] R. Siegel, Transient thermal effects of radiant energy in translucent materials, ASME J. Heat Transfer 120 (1998) 4–23.

[12] S. Andre, A. Degiovanni, A new way of solving transient radiative–conductive heat transfer problems, ASME J. Heat Transfer 120 (1998) 943–955.

[13] L.A. Tarshis, S.O. Hara, R. Viskanta, Heat transfer by simutaneous conduction and radiation for two absorbing media in intimate contact, Internat. J. Heat Mass Transfer 12 (1969) 333–346.

[14] C.H. Ho, M.N. Ozisik, Combined conduction and radiation in a two-layer planar medium with flux boundary condition, Numer. Heat Transfer 11 (1987) 321–340.

[15] R. Siegel, Two-flux green's function analysis for transient spectral radiation in a composite, AIAA J. Thermophys. Heat Transfer 10 (1996) 681–688.

[16] R. Siegel, Transient thermal analysis of parallel translucent layers by using green's functions, AIAA J. Thermophys. Heat Transfer 13 (1999) 10–17.

[17] C.F. Tsai, G. Nixon, Transient temperature distribution of a multilayer composite wall with effects of internal thermal radiation and conduction, Numer. Heat Transfer 10 (1986) 95–101.

[18] V.P. Timoshenko, M.G. Trenev, A method for evaluating heat transfer in multilayered semitransparent materials, Heat Transfer Soviet Res. 18 (1986) 44–57.

[19] R. Siegel, C.M. Spuckler, Variable refractive index effects on radiation in semitransparent scattering multilayered regions, AIAA J. Thermophys. Heat Transfer 7 (1993) 624–630.

[20] H.P. Tan, J.F. Luo, X.L. Xia, Transient coupled radiation and conduction in a three-layer composite with semitransparent specular surfaces and interfaces, ASME J. Heat Transfer, to be published.

[21] J.F. Luo, X.L. Xia, H.P. Tan, T.W. Tong, Transient coupled radiative and conductive heat transfer in a three-layer composite with opaque specular surfaces and semitransparent specular interfaces, AIAA J. Thermophys. Heat Transfer, to be published.

[22] H.P. Tan, L.M. Ruan, X.L. Xia, Q.Z. Yu, T.W. Tong, Transient coupled radiative and conductive heat transfer in an absorbing, emitting and scattering medium, Internat. J. Heat Mass Transfer 42 (1999) 2967–2980.